1 **Anti-CRISPR phages cooperate to overcome CRISPR-Cas immunity**

2

3

4

5

6 Mariann Landsberger[1], Sylvain Gandon[2], Sean Meaden[1], Hélène Chabas[1§], Angus

7 Buckling[1], Edze R. Westra[1*] and Stineke van Houte[1*]

8

9

10 [1] ESI and CEC, Biosciences, University of Exeter, Cornwall Campus, Penryn TR10

11 9EZ, UK.

12 [2] CEFE UMR 5175, CNRS Université de Montpellier Université Paul-Valéry Montpellier

13 EPHE, 34293 Montpellier Cedex 5, France.

14 [§] Current address: CEFE UMR 5175, CNRS Université de Montpellier Université Paul-

15 Valéry Montpellier EPHE, 34293 Montpellier Cedex 5, France.

16 * Correspondence: westra.edze@gmail.com, vanhoute.stineke@gmail.com.

17

18

19 **Highlights**

20   • Bacteria with CRISPR immunity remain partially resistant to Acr-phage

21   • Sequentially infecting Acr phages cooperate to overcome CRISPR resistance

22   • Acr-phage epidemiology depends on the initial phage density

23   • CRISPR resistant bacteria can drive Acr phages extinct

24

25 **eTOC blurb**

26 Some phages encode Acr proteins that block bacterial CRISPR-Cas immune systems.

27 Although CRISPR-Cas can clear the first infection, this Acr-phage still suppresses the

28 host immune system, which can be exploited by other Acr-phages. This is critical for

29 Acr-phage amplification, but this "cooperation" only works beyond a critical Acr-phage

30 density threshold.

Summary

Some phages encode anti-CRISPR (*acr*) genes, which antagonize bacterial CRISPR-Cas immune systems by binding components of its machinery, but it is less clear how deployment of these *acr* genes impacts phage replication and epidemiology. Here we demonstrate that bacteria with CRISPR-Cas resistance are still partially immune to Acr-encoding phage. As a consequence, Acr-phages often need to cooperate in order to overcome CRISPR resistance, with a first phage taking down the host CRISPR-Cas immune system to allow a second Acr-phage to successfully replicate. This cooperation leads to epidemiological tipping points in which the initial density of Acr-phage tips the balance from phage extinction to a phage epidemic. Furthermore, both higher levels of CRISPR-Cas immunity and weaker Acr activities shift the tipping points towards higher phage densities. Collectively these data help to understand how interactions between phage-encoded immune suppressors and the CRISPR systems they target shape bacteria-phage population dynamics.

Keywords: CRISPR-Cas, bacteria, phage, partial resistance, immunosuppression, anti-CRISPR, epidemiology, tipping points, bifurcation, Allee effect

Introduction

Bacteria evolve CRISPR-Cas immunity against bacteriophage (phage) by inserting phage-derived sequences into CRISPR loci on the host genome (Barrangou et al. 2007). Processed transcripts of CRISPR loci guide CRISPR-associated (Cas) surveillance complexes and effector nucleases to detect and destroy complementary genomes of re-infecting phages (Brouns et al. 2008; Garneau et al. 2010). It has been demonstrated that evolution of CRISPR immunity in bacterial populations can drive rapid phage extinction (van Houte et al. 2016). In the face of this strong selection pressure, many phages have evolved to encode anti-CRISPR (*acr*) genes (Bondy-Denomy et al. 2013; Pawluk et al. 2014; Pawluk et al. 2016a), which antagonize CRISPR immune systems of their bacterial hosts by inhibiting CRISPR surveillance complexes or effector nucleases (Bondy-Denomy et al. 2015; Pawluk et al. 2016b; Wang et al. 2016; Wang et al. 2016; Chowdhury et al. 2017; Dong et al. 2017; Guo et al. 2017; Harrington et al. 2017; Hynes et al. 2017; Pawluk et al. 2017; Peng et al. 2017; Rauch et al. 2017; Shin et al. 2017; Yang et al. 2017; Hong et al. 2018). These *acr* genes were first identified in temperate *Pseudomonas* phages (Bondy-Denomy et al. 2013) and can rescue phage from CRISPR-mediated extinction (van Houte et al.

67 2016). However, previously reported data suggests that their ability to block CRISPR

68 resistance is imperfect, and that some Acrs are more potent than others (Bondy-

69 Denomy et al. 2013). For example, phage encoding AcrF1 had greater levels of

70 infectivity on CRISPR resistant hosts compared to phage encoding AcrF4, but in all

71 cases Acr-phage infectivity was highest on hosts lacking CRISPR-Cas immunity

72 (Bondy-Denomy et al. 2013). While these data suggest that CRISPR immunity

73 provides partial resistance against Acr-phage infection, it has remained unclear how

74 these patterns of partial resistance impact the ability of Acr-phage to replicate and

75 amplify. Here we demonstrate that Acr-phages need to cooperate in order to overcome

76 partial resistance of CRISPR immune hosts. This requirement for cooperation has

77 important epidemiological consequences as it causes Acr-phages to be driven extinct

78 if their initial titers are below a critical threshold value, but allows them to amplify when

79 their titers exceed this threshold.

80

81 ## Results

82 **CRISPR-Cas confers partial immunity to Acr-phages**

83 To investigate the consequences of the previously observed partial resistance of

84 CRISPR immune bacteria against Acr-phages, we expressed AcrF1 (from phage

85 JBD30) and AcrF4 (from phage JBD26) in an isogenic phage DMS3*mvir* background,

86 which lacks an endogenous AcrF but is closely related to both parental phages.

87 Consistent with previous observations (Bondy-Denomy et al. 2013), EOP assays with

88 DMS*mvir*-AcrF1 and DMS3*mvir*-AcrF4 confirmed partial immunity of CRISPR-

89 resistant hosts to these Acr-phages and demonstrated that Acrs differ in their ability to

90 block CRISPR resistance, with AcrF1 being a more potent suppressor of CRISPR

91 resistance than AcrF4 (**Fig. 1a**). As expected, EOPs of Acr-phages on WT hosts were

92 higher compared to ancestral phage DMS3*mvir*, which is *a priori* targeted by one

93 spacer of the WT PA14 CRISPR-Cas system, but lower than those of phage DMS3*vir*,

94 which is not *a priori* targeted by the WT CRISPR-Cas system (**Fig. 1a**). Furthermore,

95 EOPs decreased when hosts carried two or five (hereafter named "BIM2" and "BIM5",

96 Bacteriophage Insensitive Mutant) targeting spacers, presumably because this

97 increases the proportion of surveillance complexes that target the phage (in addition

98 to the targeting spacers, all bacteria encode 35 non-targeting spacers). Furthermore,

99 competition between CRISPR-resistant and sensitive bacteria showed that in the

100 presence of Acr-phages CRISPR resistance provides a fitness advantage (**Fig. 1b**;

101 $F_{1,53}$ = 193.98, p<0.0001), which is consistent with the observation that targeting

102 spacers provide partial resistance to Acr-phage.

3

The size of the initial Acr-phage inoculum determines the epidemiological outcome

While full CRISPR resistance can drive phages extinct (van Houte et al. 2016), the phage epidemiology associated with partial resistance to Acr-phages is unclear. We explored this by measuring phage amplification following infection of CRISPR-resistant hosts. Whereas phage always reached similar titers when amplified for 24 hours on CRISPR-KO hosts, independent of the initial phage amount (**Fig. 2a-c**), phage amplification on WT bacteria (one targeting spacer) was dependent on the initial phage amount, with phage DMS3*mvir* amplifying exclusively beyond a threshold of around 10^6 pfus (**Fig. 2d-f**). For the Acr-phages this effect was even stronger on BIM2 (two targeting spacers) and BIM5 (5 targeting spacers) hosts, revealing epidemiological tipping points that depend both on the level of host resistance and the strength of the Acr (**Fig. 2g-l**). DMS3*mvir*-AcrF1 could only cause an epidemic on BIM2 if the initial amount of phage exceeded a threshold of ~10^5 pfus, and was driven extinct below this threshold (**Fig. 2h**), and for DMS3*mvir*-AcrF4 approximately 100-fold more phage was necessary to cause an epidemic (**Fig. 2i**). On BIM5 the tipping point shifted to approximately 10-fold higher phage titers for both Acr-phages (**Fig. 2k,l**).

Epidemiological tipping points in Acr-phage amplification are not due to phage evolution

Given that phage epidemics only occurred when bacterial cultures were infected with higher amounts of phage, we hypothesized they might be caused by rare phage mutants that "escape" (partial) CRISPR resistance due to mutations in their target sequence ("protospacer") (Antia et al. 2003; Deveau et al. 2008; Semenova et al. 2011; Jiang et al. 2013; van Houte et al. 2016). To test this, we sequenced phage that was isolated from the observed epidemics on WT, BIM2 and BIM5 following infection with 10^8 pfus (i.e. from Fig. 2d-f,h,i,k,l). This showed that the epidemic caused by control phage DMS3*mvir* on WT bacteria was indeed caused by phage that carried a mutated protospacer (i.e. mutation in the seed and PAM region) (**Fig. S1a**). However, in the context of Acr-phage, we found only one example, namely that of DMS3*mvir*-AcrF4 on PA14 WT, where the epidemic was associated with a protospacer mutation (**Fig. S1a**). For all other Acr-phage epidemics, protospacer SNP frequencies were similar to those of the ancestral phage (**Fig. S1a**). In these cases we could also not detect any differences in the ability of evolved and ancestral phages to amplify on the CRISPR-resistant hosts they were isolated from (**Fig. S1b**). Therefore, unless the Acr is weak and the host carries only one spacer, phage evolution cannot explain the observed epidemiological tipping points of Acr-phages.

4

140

Acr-phage amplification is density-dependent

142   Having ruled out that the observed tipping points by Acr-phage are the result of escape

143   phage evolution, we hypothesized that the density of Acr-phage may determine the

144   observed tipping points. To test this hypothesis, we examined whether amplification of

145   Acr-phage was density-dependent without altering the initial amount of phage. This

146   was done by measuring amplification of the same initial amount of phage on different

147   volumes of bacterial host culture, generating a High Phage-Density (HPD) condition

148   (small volume), and a Low Phage-Density (LPD) condition (large volume). Phage

149   amplification was greater on CRISPR-KO hosts under LPD conditions compared to

150   HPD conditions, simply because the bacterial densities are constant across the

151   treatments and the large volume therefore contains proportionally more bacteria on

152   which the phage can replicate (**Fig. 3**; $F_{1,22}$ = 10.54, p < 0.01). However, when Acr-

153   phages were amplified on CRISPR-resistant hosts (BIM2), the greatest level of

154   amplification was observed under HPD conditions (**Fig. 3**; $F_{1,22}$ = 59.68, p < 0.0001),

155   demonstrating that Acr-phage amplification is indeed positively density-dependent.

156   Furthermore, the level of amplification of Acr-phages on this CRISPR-resistant host

157   was independent of the presence of high amounts of phage DMS3*mvir*, which lacks

158   an *acrF* gene, demonstrating that the observed density-dependence is specifically

159   linked to the density of *acr* genes, and cannot be explained by saturation of CRISPR-

160   Cas complexes with targeted phage genomes (**Fig. S2**).

161

Epidemiological tipping points can result from cooperation between sequentially infecting Acr-phages

164   The observed density-dependent phage amplification suggested that Acr-phages may

165   cooperate in order to successfully amplify. For example, if co-infections were required

166   to effectively suppress host resistance, epidemiological tipping points could

167   correspond to parasite densities where co-infections become common (Regoes et al.

168   2002). However, this hypothesis is unlikely to explain our results, because the tipping

169   points occurred at multiplicity of infection (MOI) values where co-infections are

170   expected to be rare (e.g. MOI~0.06 for DMS3*mvir*-AcrF1 on BIM2). To explore what

171   factors may cause the observed epidemiological tipping points at low MOIs and in the

172   absence of phage evolution, we generated a theoretical model (**Supplemental Data**)

173   that accounts for the efficacy ρ of CRISPR resistance in the bacteria (ρ increases with

174   the number of spacers targeting the phage) as well as the efficacy ϕ of Acr in the

175   phage (consistent with the EOP data). In this form, the model predicts that upon

176   infection of 10^6 CRISPR-resistant bacteria phage expressing a strong Acr can always

5

177 amplify, regardless of the initial phage density (**Fig. S3**, ϕ=0.67, purple line), whereas

178 phage with a weak Acr can never amplify (**Fig. S3**, ϕ=0.6 and ϕ=0.5, magenta and

179 green lines respectively; grey lines correspond to the initial amount of phage and

180 values below this line indicate a lack of phage amplification). Given that these model

181 predictions are inconsistent with our experimental data, we then extended the model

182 by incorporating the assumption that during failed infections some Acr is produced that

183 causes the surviving host to enter a "suppressed" state ("S"). This immunosuppression

184 decreases the efficacy of host resistance and allows following phages to exploit these

185 bacteria (**Fig. 4a**). Crucially, if the immunosuppressed state is assumed, the model

186 predicts epidemiological tipping points and, in accordance with our empirical data,

187 these tipping points occur at MOIs far below 1 (**Fig. 4b**). Besides, our experimental

188 observations that the position of the tipping points shifts when Acrs are weaker or host

189 resistance is stronger (**Fig. 2**) are fully explained by our model when we vary the effect

190 of the efficacy ϕ of the Acr in the phage (**Fig. 4b**), or the efficacy ρ of CRISPR

191 resistance in the bacteria (i.e., the number of spacers in the host targeting the phage,

192 **Fig. 4c**). Moreover, longer periods of immunosuppression shift the tipping points to

193 lower phage densities, as it increases the probability that a host will be re-infected

194 when it is still in the immunosuppressed state (**Fig. 4d,** indicated by γ). This model

195 therefore predicts that Acr-phage infections can cause CRISPR-resistant bacteria to

196 become immunosuppressed, allowing cooperation between sequentially infecting Acr-

197 phages to overcome CRISPR immunity, which is a critical factor in determining

198 whether Acr-phages can amplify.

199

200 **Unsuccessful infections by Acr-phages cause CRISPR-resistant hosts to**

201 **become immunosuppressed**

202 To validate this model we tested the key assumption that unsuccessful infections by

203 Acr-phages cause CRISPR-resistant hosts to become immunosuppressed. To this

204 end, we pre-infected BIM2 and BIM5 bacteria with Acr-phage at a low MOI (~0.3) and

205 subsequently washed away all remaining phages from the culture. We then measured

206 the relative transformation efficiency (RTE) of the surviving cells by transforming pre-

207 infected bacteria with either a CRISPR-targeted plasmid (T) or a non-targeted plasmid

208 (NT). For all phage treatments, the RTE of pre-infected CRISPR-KO bacteria and non-

209 infected controls were not significantly different, as expected (**Fig. 5**; $F_{1,51} = 1.12$, p =

210 0.35). However, when BIM2 or BIM5 bacteria were pre-infected with phage DMS3*mvir*-

211 AcrF1, the RTE increased significantly compared to the DMS3*mvir* and no-phage

212 controls (**Fig. 5**; BIM2: $F_{1,17} = 26.82$, p < 0.0001, BIM5: $F_{1,20} = 20.16$, p < 0.0001),

213 demonstrating lasting immunosuppression of CRISPR-resistant hosts following an

6

214 unsuccessful infection with Acr-phage. Consistent with its weaker Acr activity, lasting

215 immunosuppression following infection with DMS3*mvir*-AcrF4 was only observed in

216 BIM2 (**Fig. 5**; $F_{1,17}$ = 5.26, p<0.05) and not BIM5 ($F_{1,20}$ = 2.07, p = 0.15).

217

218 **Discussion**

219 The discovery of Acr proteins has been a major breakthrough in CRISPR-Cas research

220 (Bondy-Denomy et al. 2013). Since their initial discovery much progress has been

221 made towards biochemical characterization of Acrs and the unraveling of their

222 molecular mode of action. Here we study the population dynamics associated with

223 CRISPR-Acr interactions and demonstrate that the initial density of Acr-phages that

224 infect bacteria with partial CRISPR resistance determines whether phages go extinct

225 or amplify. We ruled out that the need for high Acr-phage densities is simply linked to

226 the evolution of phage escape mutations. Instead, the observed epidemiological

227 tipping points can be primarily explained by long-term suppression of CRISPR

228 resistance following an unsuccessful infection, which is consistent with the slow

229 dissociation kinetics of Acr-Cas protein complexes (Chowdhury et al. 2017). Modeling

230 the temporal phage and host population dynamics shows that during the initial stages

231 of infection Acr-phage densities decline due to the high proportion of unsuccessful

232 infections (Supplemental Information and **Fig. S4ab**). However, as the densities of

233 immunosuppressed hosts increase a greater proportion of infections becomes

234 successful. If the initial densities of Acr-phages are high enough, densities of

235 immunosuppressed hosts reach a critical threshold where the amount of new Acr-

236 phages that are produced from successful infections outweighs the loss of Acr-phages

237 due to unsuccessful infections, causing the epidemic to take off (**Fig. S4b**). If this

238 critical threshold is not reached, the Acr-phage goes extinct and immunosuppressed

239 hosts revert to their resistant state (**Fig. S4a**).

240 The long-term immunosuppression following a failed infection of Acr-phage is

241 cooperative in that it provides a benefit to Acr-phages that sequentially infect the same

242 host to overcome CRISPR resistance. Future studies aimed at measuring the costs

243 and benefits associated with phage-encoded Acr genes and their natural ecology will

244 be critical to understanding the evolutionary drivers and stability of Acr-phage

245 cooperation (Sachs et al. 2004, West et al 2007). Specifically, it is unclear the extent

246 to which lasting immunosuppression evolved because of the indirect fitness benefits

247 associated with the enhanced infection success of clone mates in the population, or

248 whether it is primarily a by-product of the direct individual-level benefits of suppressing

249 the host immune system.

250   As discussed above, amplification of Acr-phages on CRISPR-resistant bacteria

251   was found to occur only if the initial Acr-phage densities were above a certain threshold

252   value, which is determined both by the strength of the Acr and the resistance level of

253   the host. Below this threshold CRISPR-resistant bacteria drive phage to extinction,

254   despite the phage-encoded Acr. In general, positive density-dependent fitness effects

255   are thought to play an important role in various ecological contexts, such as species

256   invasions, extinctions and disease epidemics (Courchamp et al. 1999; Stephens et al.

257   1999). Existing theory predicts that parasite density-dependent tipping points in

258   disease epidemics can occur when the infection dynamics of an individual host

259   depends on the parasite dose, for example when there is a threshold in the number of

260   co-infecting parasites that are required to establish a successful infection (Regoes et

261   al. 2002). This work shows that epidemiological tipping points can also take place

262   under conditions where parasite densities are too low for co-infections to be common

263   if unsuccessful infections leave behind an immunosuppressed host. The profound

264   epidemiological consequences that were found to be associated with lasting

265   immunosuppression in our empirical system warrant future studies to explore whether

266   similar effects play a role in the epidemiology of other infectious diseases.

267

280

281   **Author contributions**

282   Conceptualization, ERW, SvH, AB; Methodology, ERW, SvH, ML, SG; Investigation,

283   ML, HC, SvH, ERW; Formal Analysis, ML, SM, SvH, ERW, SG; Writing – Original Draft,

284   SvH, ERW; Writing – Review & Editing, SvH, ERW, ML, SG, AB; Funding Acquisition,

285   ERW, SvH; Supervision, ERW, SvH.

286

287 **Declaration of interest**

288 The authors declare no competing interests.

289

290 **References**

291 Antia, R., Regoes, R. R., Koella, J. C. & Bergstrom, C. T. (2003) The role of evolution
292 in the emergence of infectious diseases. Nature 426, 658-661.

293

294 Barrangou, R. et al. (2007) CRISPR provides acquired resistance against viruses in
295 prokaryotes. Science 315, 1709-12.

296

297 Bondy-Denomy, J. et al. (2015) Multiple mechanisms for CRISPR-Cas inhibition by
298 anti-CRISPR proteins. Nature 526, 136-139.

299

300 Bondy-Denomy, J., Pawluk, A., Maxwell, K. L. & Davidson, A. R. (2013) Bacteriophage
301 genes that inactivate the CRISPR/Cas bacterial immune system. Nature 493, 429-432.

302

303 Brouns, SJJ. et al. (2008) Small CRISPR RNAs guide antiviral defense in prokaryotes.
304 Science 321, 960-964.

305

306 Cady, K. C., Bondy-Denomy, J., Heussler, G.E., Davidson, A.R., O'Toole, G.A. (2012)
307 The CRISPR/Cas adaptive immune system of *Pseudomonas aeruginosa* mediates
308 resistance to naturally occurring and engineered phages. J Bacteriol. 194, 5728-38.

309

310 Choi, K.H., Kumar, A., Schweizer, H.P. (2006) A 10-min method for preparation of
311 highly electrocompetent *Pseudomonas aeruginosa* cells: application for DNA fragment
312 transfer between chromosomes and plasmid transformation. J Microbiol Methods 64,
313 391-7.

314

315 Chowdhury, S. et al. (2017) Structure reveals mechanisms of viral suppressors that
316 intercept a CRISPR RNA-guided surveillance complex. Cell 169, 47-57.

317

318 Courchamp, F., Clutton-Brock, T. & Grenfell, B. (1999) Inverse density dependence
319 and the Allee effect. Trends Ecol. Evol. 14, 405-410.

320

321 Deveau, H. et al. (2008) Phage response to CRISPR-encoded resistance in
322 *Streptococcus thermophilus*. J Bacteriol 190, 1390-1400.

323

324 Dong, D. et al. (2017) Structural basis of CRISPR-SpyCas9 inhibition by an anti-
325 CRISPR protein. Nature 546, 436-439.
326
327 Garneau, JE. et al. (2010) The CRISPR/Cas bacterial immune system cleaves
328 bacteriophage and plasmid DNA. Nature 468, 67-71.
329
330 Guo, T. W. et al. (2017) Cryo-EM structures reveal mechanism and inhibition of DNA
331 targeting by a CRISPR-Cas surveillance complex. Cell 171, 414-426.
332
333 Harrington, L. B. et al. (2017) A broad-spectrum inhibitor of CRISPR-Cas9. Cell 170,
334 1224-1233.
335
336 Hong, S. et al. (2018) CRISPR RNA and anti-CRISPR protein binding to the
337 *Xanthomonas albilineans* Csy1-Csy2 heterodimer in the type I-F CRISPR-Cas system.
338 J Biol Chem. doi: 10.1074/jbc.RA117.001611.
339
340 Hynes, A. P. et al. (2017) An anti-CRISPR from a virulent streptococcal phage inhibits
341 *Streptococcus pyogenes* Cas9. Nat Microbiol. 2, 1374-1380.
342
343 Jiang, W. et al. (2013) Dealing with the evolutionary downside of CRISPR immunity:
344 bacteria and beneficial plasmids. Plos Genet 9, e1003844.
345
346 Pawluk, A., Bondy-Denomy, J., Cheung, V.H., Maxwell, K.L., Davidson, A.R. (2014) A
347 new group of phage anti-CRISPR genes inhibits the type I-E CRISPR-Cas system of
348 *Pseudomonas aeruginosa*. MBio 5:e00896.
349
350 Pawluk, A. et al. (2016a) Inactivation of CRISPR-Cas systems by anti-CRISPR
351 proteins in diverse bacterial species. Nat Microbiol. 1:16085..
352
353 Pawluk, A. et al. (2016b) Naturally occurring off-switches for CRISPR-Cas9. Cell 167,
354 1829-1838.
355
356 Pawluk, A. et al. (2017) Disabling a Type I-E CRISPR-Cas nuclease with a
357 bacteriophage-encoded anti-CRISPR protein. MBio 8: e01751-17.
358

359   Peng, R. et al. (2017) Alternate binding modes of anti-CRISPR viral suppressors
360   AcrF1/2 to Csy surveillance complex revealed by cryo-EM structures. Cell Res. 27,
361   853-864.

363   Rauch, B. J. et al. (2017) Inhibition of CRISPR-Cas9 with bacteriophage proteins. Cell
364   168, 150-158.

366   Regoes, R. R., Ebert, D. & Bonhoeffer, S. (2002) Dose-dependent infection rates of
367   parasites produce the Allee effect in epidemiology. Proc. Biol. Sci. 269, 271-279.

369   Sachs, J.L., Mueller, U.G., Wilcox, T.P., Bull, J.J. (2004) The evolution of cooperation.
370   Q Rev Biol. 79:135-60.

372   Semenova, E. et al. (2011) Interference by clustered regularly interspaced short
373   palindromic repeat (CRISPR) RNA is governed by a seed sequence. Proc Natl Acad
374   Sci U S A 108, 10098-10103.

376   Shin, J. et al. (2017) Disabling Cas9 by an anti-CRISPR DNA mimic. Sci Adv.
377   3:e1701620.

379   Stephens, P. A. & Sutherland, W. J. (1999) Consequences of the Allee effect for
380   behaviour, ecology and conservation. Trends Ecol. Evol 14, 401-405.

382   van Houte, S. et al. (2016) The diversity-generating benefits of a prokaryotic adaptive
383   immune system. Nature 532, 385-388.

385   Wang, J. et al. (2016) A CRISPR evolutionary arms race: structural insights into viral
386   anti-CRISPR/Cas responses. Cell Res. 26, 1165-1168.

388   Wang, X. et al. (2016) Structural basis of Cas3 inhibition by the bacteriophage protein
389   AcrF3. Nat Struct Mol Biol. 23, 868-70.

391   West, S.A., Griffin, A.S., Gardner, A. (2007). Evolutionary explanations for
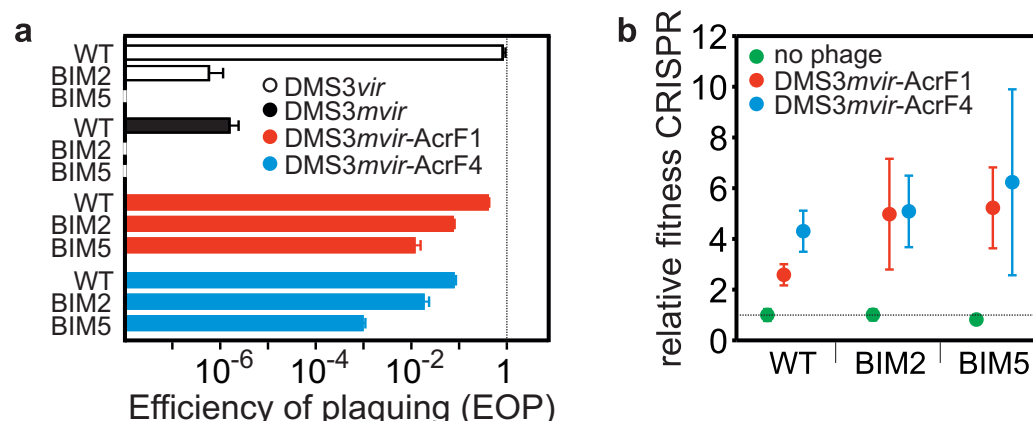392   cooperation. Curr Biol. 17:R661-72.

394   Westra, E. R. et al. (2015) Parasite exposure drives selective evolution of constitutive
395   versus inducible defense. Curr Biol. 25, 1043-9.

396

397   Yang H, Patel DJ. (2017) Inhibition mechanism of an Anti-CRISPR suppressor AcrIIA4

398   targeting SpyCas9. Mol Cell. 67, 117-127.

399

Figures

Figure 1. CRISPR-resistant hosts are partially immune to phage encoding an anti-CRISPR. **(a)** Efficiency of plaquing (EOP) of DMS3*vir* (white bars) on PA14 WT (completely sensitive to DMS3*vir*), BIM2 (1 spacer targeting DMS3*vir*) and BIM5 (4 spacers targeting DMS3*vir*); EOP of DMS3*mvir* (black bars), DMS3*mvir*-AcrF1 (red bars) and DMS3*mvir*-AcrF4 (blue bars) on PA14 WT (1 spacer targeting DMS3*mvir*, DMS3*mvir*-AcrF1 and DMS3*mvir*-AcrF4), BIM2 (2 spacers targeting DMS3*mvir*, DMS3*mvir*-AcrF1 and DMS3*mvir*-AcrF4) and BIM5 (5 spacers targeting DMS3*mvir*, DMS3*mvir*-AcrF1 and DMS3*mvir*-AcrF4). Each experiment was performed as 6 independent replicates. Error bars represent 95% confidence intervals (c.i.). **(b)** Relative fitness of CRISPR-resistant bacteria on PA14 WT, BIM2 and BIM5 in the absence of phage (green data points) or in the presence of phage DMS3*mvir*-AcrF1 (red data points) or phage DMS3*mvir*-AcrF4 (blue data points). Each experiment was performed as 6 independent replicates, error bars represent 95% c.i.

13
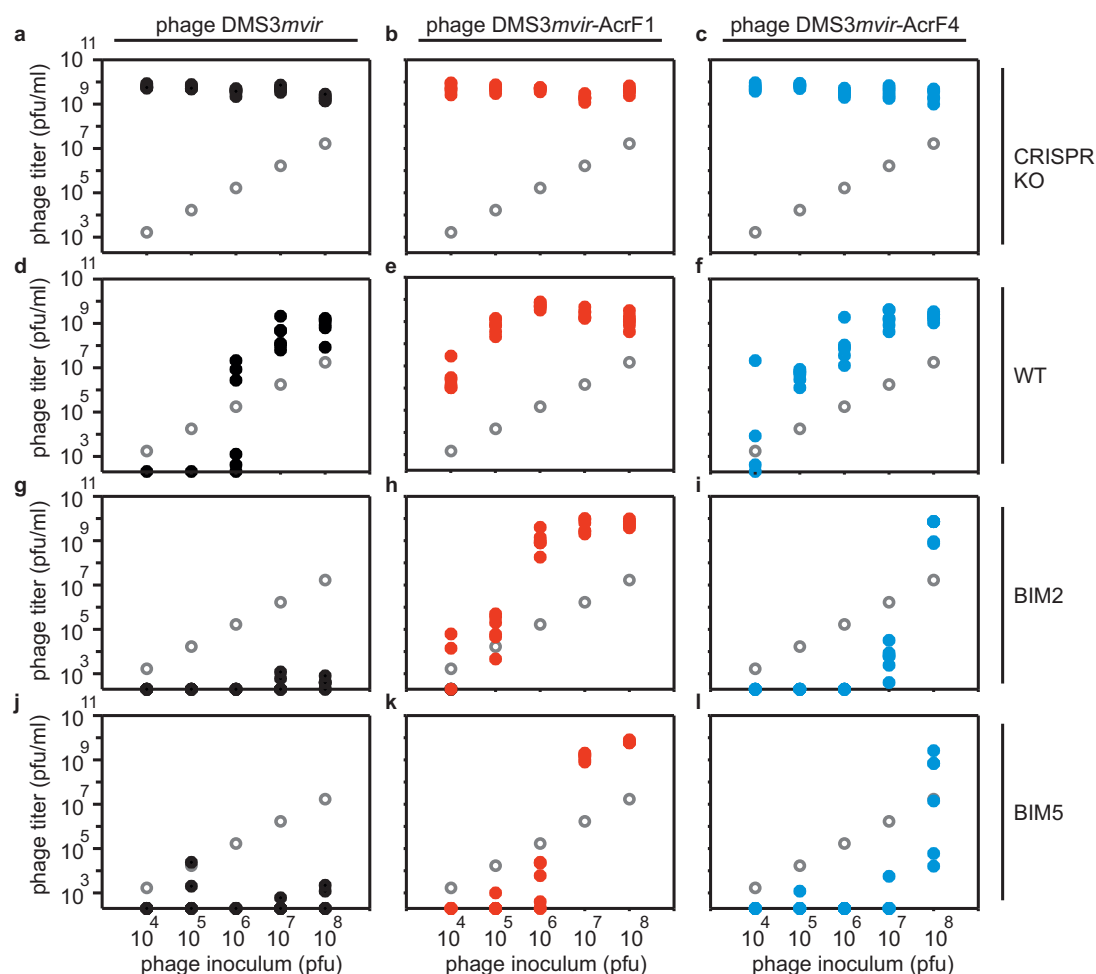
Figure 2. Partial immunity to phages encoding anti-CRISPR causes epidemiological tipping points that are phage density-dependent. Viral titers at 24 hours post-infection (hpi) with DMS3*mvir* (**a,d,g,j**), DMS3*mvir*-AcrF1 (**b,e,h,k**) or DMS3*mvir*-AcrF4 (**c,f,i,l**) of PA14 CRISPR-KO (**a-c**), WT (**d-f**), BIM2 (**g-i**) or BIM5 (**j-l**). Grey circles indicate the phage titers (pfu/ml) at the start of the experiment (corresponding to the addition of $10^4, 10^5, 10^6, 10^7$ or 10^8 pfus). Colored data points represent phage titers at 24 hpi; each data point represents an independent biological replicate (*n*=6). The limit of detection is 200 pfu/ml.

14
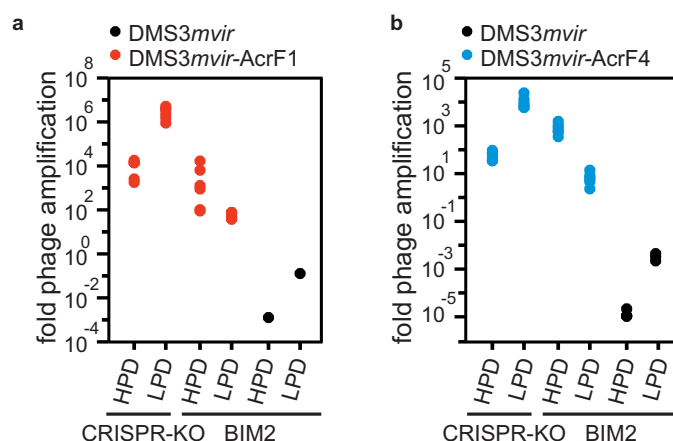
Figure 3. Acr-phage amplification is density-dependent. (**a**) Fold phage amplification at 24 hpi with 10^6 pfus DMS3*mvir* (black data points) or DMS3*mvir*-AcrF1 (red data points) of PA14 CRISPR-KO (sensitive) or BIM2 under either high phage densities (HPD, 6 ml culture) or low phage densities (LPD, 600 ml culture). (**b**) Fold phage amplification at 24 hpi with 10^8 pfus DMS3*mvir* (black data points) or DMS3*mvir*-AcrF4 (blue data points) of PA14 CRISPR-KO (sensitive) or BIM2 under either HPD or LPD; each data point represents an independent biological replicate (*n*=6). The limit of detection is 200 pfu/ml.

15
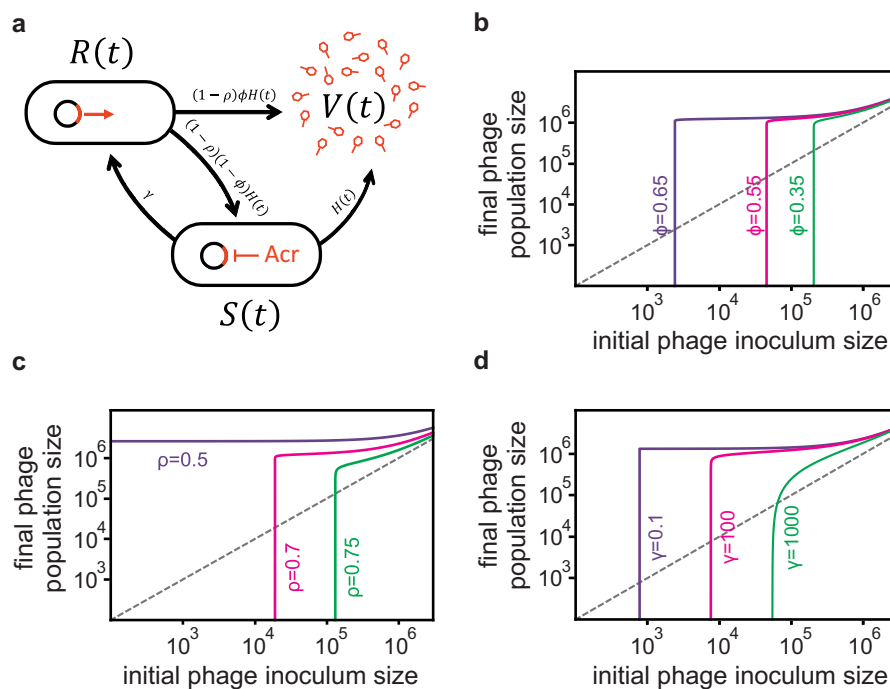
Figure 4. Lasting immunosuppression following unsuccessful Acr-phage infections can lead to epidemiological tipping points. (**a**) Infection model of the Acr-phage (see details of the model in Supplementary Information). The parameter $H(t)=\alpha V(t)$ refers to the rate at which bacteria are infected by free phage particles. (**b**) Effect of initial Acr-phage inoculum density on the phage density at 24 hpi for different values of Acr efficacy (ϕ = 0.65 (purple), ϕ = 0.55 (magenta) and ϕ = 0.35 (green)); other parameter values: B = 5, α = 0.001, ρ = 0.7, γ = 20. (**c**) Effect of initial Acr-phage inoculum density on the phage density after 24h of incubation for different values of CRISPR efficacy (ρ = 0.5, 0.7 and 0.75; purple, magenta, green respectively); other parameter values: B = 5, α = 0.001, ϕ = 0.6, γ = 20. (**d**) Effect of initial Acr-phage inoculum density on the phage density after 24h of incubation for different values of the duration of the immunosuppressive state (γ = 0.1, 100 and 1000; purple, magenta, green respectively); other parameter values: B = 5, α = 0.001, ϕ = 0.65, ρ = 0.7. In all graphs, grey lines correspond to the initial amount of phage and values below this line indicate a lack of phage amplification.

16
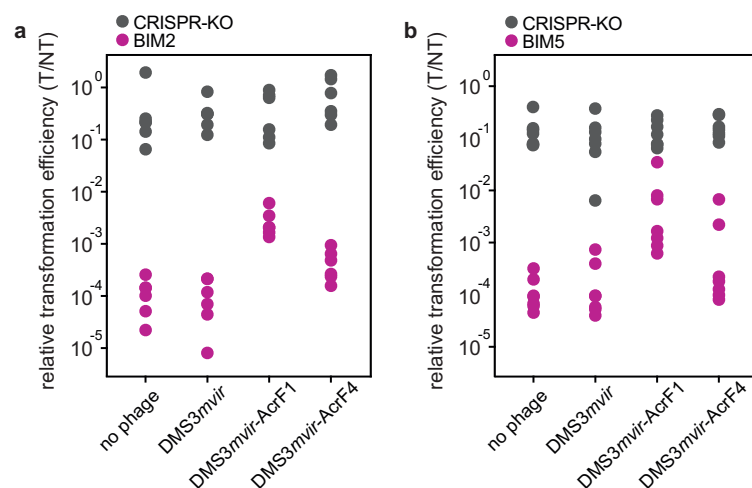
Figure 5. Infection with Acr-phage lead to long-term immunosuppression of CRISPR-resistant hosts. (**a**) Relative transformation efficiencies (RTE) of CRISPR-KO (grey data points) or BIM2 (purple data points) pre-infected with $1.6*10^9$ pfus of either DMS3*mvir*, DMS3*mvir*-AcrF1 or DMS3*mvir*-AcrF4, or not phage-infected. Each data point represents an independent biological replicate (*n*=6). (**b**) RTE of CRISPR-KO (grey data points) or BIM5 (purple data points) pre-infected as described for (a). Each data point represents an independent biological replicate (*n*=7).

459   **Materials and methods**

460

461   *Bacterial strains*

462   *P. aeruginosa* UCBPP-PA14 (WT; carrying one spacer targeting DMS3*mvir*) and *P.*

463   *aeruginosa* UCBPP-PA14 *csy3::LacZ* (referred to as CRISPR-KO, which carries a

464   disruption of an essential *cas* gene and can therefore not evolve CRISPR immunity),

465   have been described in (Cady et al. 2012; Westra et al. 2015; van Houte et al. 2016).

466   The BIM2 strain (carrying two spacers targeting DMS3*mvir*) has been described in

467   (Westra et al. 2015). The BIM5 strain (carrying 5 spacers targeting DMS3*mvir*) was

468   generated by challenging PA14 BIM2 bacteria with escape phage in multiple rounds,

469   giving rise to BIM3, BIM4 and finally BIM5.

470

471   *Phage strains and generation of recombinant phages*

472   Phages DMS3*vir*, DMS3*mvir* and DMS3*mvir*-AcrF1 have been previously described in

473   refs. (Cady et al. 2012; Bondy-Denomy et al. 2013; van Houte et al. 2016). Phage

474   DMS3*mvir*-AcrF4, which carries the anti-CRISPR gene *acrF4* (formerly JBD26-37),

475   was made by generating a plasmid possessing the *acrF4* gene flanked by regions of

476   homology from JBD30 (which are nearly identical to DMS3*m*). DMS3*m* was used to

477   infect cells possessing this plasmid and recombinants possessing *acrF4* were selected

478   for. This phage (DMS3*m*-AcrF4) was then made virulent via C-repressor deletion as in

479   (Cady et al. 2012). Genome assemblies of DMS3*mvir*-AcrF1 and DMS3*mvir*-AcrF4

480   used in this study can be found under GenBank accession number XXXXX.

481

482   *Efficiency of Plaquing (EOP) assays*

483   EOP assays were carried out on plates containing LB with 1.5% agar. A mixture of

484   molten soft LB agar (0.5%), 300 µl of bacteria (grown O/N in M9 growth medium

485   supplemented with 0.2% glucose) and 100 µl of serially diluted phage was poured on

486   top of the hard agar layer. Plates were incubated O/N at 37 ºC and plaques were

487   enumerated the next day.

488

489   *Competition assays to measure CRISPR-associated fitness*

490   Competition experiments were performed in glass vials in 6 ml M9 medium (22 mM

491   Na_2HPO_4; 22 mM KH_2PO_4; 8.6 mM NaCl; 20 mM NH_4Cl; 1 mM $MgSO_4$; 0.1 mM $CaCl_2$)

492   supplemented with 0.2% glucose. Competition experiments were initiated by

493   inoculating 1:100 from a 1:1 mixture of overnight cultures (grown in M9 medium + 0.2%

494   glucose) of the CRISPR-resistant strain (either WT, BIM2 or BIM5) and the sensitive

495   CRISPR-KO strain. To each microcosm 10^4 plaque forming units (pfus) of either

496   DMS3*mvir*-AcrF1 or DMS3*mvir*-AcrF4 phage was added, and each treatment was
497   performed in six independent replicates. At 0 and 24 hours after the start of the
498   competition experiment samples were taken and cells were serially diluted in M9 salts
499   (22 mM Na_2HPO_4; 22 mM KH_2PO_4; 8.6 mM NaCl; 20 mM NH_4Cl) and plated on LB
500   agar supplemented with 50 µg·ml^{-1} X-gal (to allow discrimination between CRISPR-
501   resistant (white) and sensitive CRISPR-KO (blue) bacteria). For all competitions, a
502   control competition experiment was performed in the absence of phage. For all
503   competitions, relative frequencies of the CRISPR-resistant strains were determined
504   and used to calculate the relative fitness (rel. fitness = [(fraction strain A at t=x) * (1 –
505   (fraction strain A at t=0))] / [(fraction strain A at t=0) * (1 – (fraction strain A at t=x)]).
506   These values were used for student t-test or ANOVA. All subsequent statistical
507   analyses were carried out using R.
508
509   *Infection assays in liquid medium*
510   Infection assays were performed in glass vials by inoculating 6 ml M9 medium
511   supplemented with 0.2% glucose with 60 µl (app. $2*10^7$ colony forming units (cfus)
512   bacteria from fresh overnight cultures (also grown in M9 medium + 0.2% glucose) of
513   either the CRISPR-KO, WT, BIM2 or BIM5 strain. To these microcosms 10^4, 10^5, 10^6,
514   10^7 or 10^8 pfus of either DMS3*mvir*, DMS3*mvir*-AcrF1 or DMS3*mvir*-AcrF4 phage were
515   added. Each treatment was performed in six independent replicates. Microcosms were
516   incubated at 37 ºC while shaking at 180 rpm. Phage was extracted at 24 hours after
517   the start of the experiment by chloroform extraction on all samples (sample: chloroform
518   10:1 v/v), and phage titers were determined by spotting isolated phage samples on a
519   lawn of CRISPR-KO bacteria.
520   For the experiment shown in **Fig. S2** the same protocol was used but with 10^8
521   pfus DMS3*mvir* added to each treatment at the start of the experiment (**Fig. S2b,d**).
522   For the infection assays in which phage densities were manipulated by using different
523   volumes of growth medium (**Fig. 3**), glass microcosms containing 6 ml M9 growth
524   medium + 0.2% glucose were used for the high phage-density (HPD) treatment. These
525   were inoculated with 60 µl (app. $2*10^7$ cfus) bacteria from fresh overnight cultures of
526   the CRISPR-KO or BIM2 strains, as above. For the low phage-density (LPD) treatment
527   Duran 1L glass bottles containing 600 ml M9 growth medium + 0.2% glucose were
528   used, which were inoculated with 6 ml (app. $2*10^9$ cfus) bacteria from the same
529   overnight cultures. To both glass vials and bottles phage was added (10^6 pfus of
530   DMS3*mvir*-AcrF1; 10^8 pfus of DMS3*mvir*-AcrF4 or 10^8 pfus of DMS3*mvir*). Glass vials
531   and bottles were incubated at 37 ºC while shaking at 180 rpm. Total phage was
532   extracted at 24 hours after the start of the experiment by chloroform extraction (sample:

19

533   chloroform 10:1 v/v), and phage titers were determined by spotting all isolated phage

534   samples on a lawn of CRISPR-KO bacteria. All experiments were performed in six

535   independent replicates.

536

537   *Deep sequencing of phages*

538   From the experiments shown in Fig. 2a-l, phage was isolated from the treatments that

539   were infected with 10^8 pfus of phage. These phages were used for a new round of

540   infection assays in liquid media (Fig. S1), effectively following the methods described

541   above, and for deep sequencing analysis. To obtain sufficient material for the latter,

542   isolated phage was amplified by plaque assay on the CRISPR-KO strain. Phage

543   samples from all replicates within a single treatment were pooled. As controls,

544   ancestral DMS3*mvir*, DMS3*mvir*-AcrF1 and DMS3*mvir*-AcrF4 phage were processed

545   in parallel. Phage genomic DNA extraction was performed with 600 µl sample at

546   approximately 10^{12} pfu/ml using the Norgen phage DNA isolation kit, following the

547   manufacturer's instructions. Barcoded Illumina Truseq Nano libraries were constructed

548   from each DNA sample with an approximately 350 bp insert size and 2 × 250 bp reads

549   generated on an Illumina MiSeq platform. Reads were trimmed using Cutadapt version

550   1.2.1 and Sickle version 1.200 and then overlapping reads merged using Flash version

551   1.2.11 to create high quality sequence at approximately 8000 × coverage of DMS3*mvir*

552   per sample. These reads were mapped to the DMS3*mvir* genomes using bwa mem

553   version 0.7.12 and allele frequencies of single nucleotide polymorphisms within viral

554   target regions quantified using samtools mpileup version 0.1.19. Further statistical

555   analyses was performed in R version 3.4.1. Sequence data are available from the

556   European Nucleotide Archive under accession number PRJEB25016 and analysis

557   scripts are available from https://github.com/s-meaden/landsberger.

558

559   *Generation of CRISPR-targeted plasmid*

560   For the long-term immunosuppression experiment (**Fig. 5**) plasmid pHERD30T was

561   used. To generate pHERD30T that was *a priori* targeted by the PA14 WT Type I-F

562   CRISPR-Cas system, the mutant plasmid pHERD30T*targ* was generated that carries

563   a 32-nt protospacer sequence flanked by a GG protospacer adjacent motif (PAM) with

564   full complementarity to spacer 1 in CRISPR locus 2 of the PA14 WT Type I-F CRISPR-

565   Cas system. This was done by ligation of oligonucleotides that upon annealing create

566   overhangs that are compatible with *Hind*III ligation (5'-

567   agcttACCGCGCTCGACTACTACAACGTCCGGCTGAT GGa-3' and 5'-

568   agcttCCATCAGCCGGACGTTGTAGTAGTCGAGCGCGGTa-3', *Hind*III overhangs in

569 small caps, protospacer sequence in capitals and PAM underlined) in the *Hind*III-
570 digested pHERD30T vector.

571

572 *Long-term immunosuppression experiment*

573 Suppression of CRISPR immunity by Acr was measured through a transformation
574 assay. CRISPR-KO, BIM2 or BIM5 bacteria (app. $5*10^9$ cfus) were either not infected
575 or infected with $1.6*10^9$ pfus DMS3*mvir*, DMS3*mvir*-AcrF1 or DMS3*mvir*-AcrF4 in 50
576 mL Falcon tubes containing 10 mL of Luria-Bertani (LB) broth, and incubated at 37 ºC
577 while shaking at 180 rpm for 2 hours. Bacteria were harvested by spinning at 3500 rpm
578 for 30 minutes, after which a sample was taken from the supernatant for chloroform
579 extraction (sample: chloroform 10:1 v/v) to quantify phage titers (data not shown). The
580 bacterial pellet was then washed twice in 1 mL of a 300 mM sucrose solution to make
581 them competent (Choi et al. 2006). Finally the pellet was resuspended in 300 µl of 300
582 mM sucrose, and 100 µl from this was used for plating on LB agar to enumerate total
583 bacterial cfus after the infection and sucrose-washing steps (data not shown). The
584 remaining 200 µl was divided in equal volumes over two eppendorf tubes, and were
585 used for electrotransformation with either plasmid pHERD30T (not targeted by
586 CRISPR-Cas; NT) or pHERD30T*targ* (targeted by CRISPR-Cas; T). Electroporated
587 bacteria were resuspended in 1 ml LB broth and incubated 1h at 37ºC at 180 rpm.
588 Bacteria were then pelleted and resuspended in 100 µl LB and plated on LB agar
589 plates containing Gentamycin (50 µg·ml^{-1}) and incubated for 16h at 37 ºC to allow
590 transformants to grow. For each of the four phage treatments the number of
591 transformants from the NT and T transformation was used to calculate the relative
592 transformation efficiency (T/NT).